Signal, Image and Video Processing (2020) 14:1189–1197
https://doi.org/10.1007/s11760-020-01657-9

ORIGINAL PAPER

An adaptive method for image restoration based on high-order total variation and inverse gradient

Dang N. H. Thanh[1] · V. B. Surya Prasath[2,3,4,5] · Le Minh Hieu[6] · Sergey Dvoenko[7]

Received: 27 May 2019 / Revised: 20 January 2020 / Accepted: 5 February 2020 / Published online: 23 February 2020

Abstract

The total variation (TV) regularization model for image restoration is widely utilized due to its edge preservation properties. Despite its advantages, the TV regularization can obtain spurious oscillations in flat regions of digital images and thus recent works advocate high-order TV regularization models. In this work, we propose an adaptive image restoration method based on a combination of first-order and second-order total variations regularization with an inverse-gradient-based adaptive parameter. The proposed model removes noise effectively and preserves image structures. Due to the adaptive parameter estimation based on the inverse gradient, it avoids the staircasing artifacts associated with TV regularization and its variant models. Experimental results indicate that the proposed method obtains better restorations in terms of visual quality as well as quantitatively. In particular, our proposed adaptive higher-order TV method obtained (19.3159, 0.7172, 0.90985, 0.79934, 0.99838) PSNR, SSIM, MS-SSIM, F-SIM, and P-SIM values compared to related models such as the TV-Bounded Hessian (18.9735, 0.6599, 0.8718, 0.73833, 0.99767), and TV-Laplacian (19.0345, 0.6719, 0.88198, 0.75405, 0.99789).

Keywords Image restoration · Image denoising · Image processing · High-order total variation · Image quality assessment

✉ Dang N. H. Thanh
hoangthanh@ueh.edu.vn; thanh.dnh.cs@gmail.com

V. B. Surya Prasath
prasatsa@uc.edu

Le Minh Hieu
hieulm@due.edu.vn

Sergey Dvoenko
dvsrge@gmail.com

1 Department of Information Systems, School of Business Information Technology, University of Economics Ho Chi Minh city, Ho Chi Minh city, Vietnam

2 Division of Biomedical Informatics, Cincinnati Children's Hospital Medical Center, Cincinnati, OH 45229, USA

3 Department of Pediatrics, University of Cincinnati College of Medicine, Cincinnati, OH, USA

4 Department of Biomedical Informatics, College of Medicine, University of Cincinnati, Cincinnati, OH 45267, USA

5 Department of Electrical Engineering and Computer Science, University of Cincinnati, Cincinnati, OH 45221, USA

6 University of Economics, The University of Danang, Danang, Vietnam

7 Department of Information Security, Institute of Applied Mathematics and Computer Science, Tula State University, Tula, Russia

1 Introduction

Image restoration [1–8] plays a vital role in automatic image processing pipelines. The goal of image restoration is to obtain noise-free images from corrupted images. Recently, there exists a variety of approaches that have been used to solve the problem [3,9,10]. Regularization [3, 10] is one of the popular mathematical tools to solve inverse problems. Among a variety of regularization models for image restoration, the total variation (TV) is the most utilized one due to its strong edge preservation properties.

The image restoration problem has various forms such as image denoising [11–20], image deblurring [21,22], image inpainting [23,24], image dehazing [25], image de-raining [26]. In this work, we concentrate on the image denoising problem for the additive Gaussian noise. To restore images degraded by the Gaussian noise, Rudin et al. [27] proposed the ROF model (Rudin–Osher–Fatemi) that is derived from the TV regularization. Although the ROF model works effectively and preserves edges well, there are still several existing issues: restoring images using the ROF model does not preserve geometrical features and can cause staircasing artifacts in flat regions. There are many methods relying on TV and its

variants that have been developed to eliminate these disadvantages. A well-known method is to replace the first-order total variation in the regularization term by the second-order (or higher-order) total variation. The second-order total variation can avoid staircasing artifacts to a certain degree, but its effectiveness for noise removal can be inferior to the first-order total variation. Hence, it is necessary to combine the advantages of the first-order and the second-order total variations with an efficient balancing weight of these regularization terms to guarantee effectiveness for noise removal and artifact elimination. In [28], a combined model named total variation bounded Hessian (TVBH) is proposed with improved restoration results compared to the TV model. However, estimating the parameters involved in the model is still an open problem.

Our contributions are to propose an adaptive model based on TVBH, to estimate the regularization parameter by multiscale capture of edges via the inverse gradient [2,23] and to propose an algorithm to solve the model based on the alternating direction method of multipliers [11,28,31]. In the experiments, we test the proposed method on synthetic as well as natural images of the Berkeley dataset (BSDS) [29]. We further compare the restoration results of the proposed method with TVBH [28], TV-Laplacian model (TVL) [30] for various noisy images. TVL [30] is a novel and effective model that combines the first-order total variation with the Laplacian regularizer. In order to assess image quality after restoration, we use the peak signal-to-noise ratio (PSNR), the structural similarity (SSIM), the multiscale structural similarity (MS-SSIM), the features similarity (F-SIM), and the perceptual similarity (P-SIM) metrics.

The rest of the paper is organized as follows. Section 2 presents the image restoration problem, the proposed method incorporating adaptive parameter estimation and the numerical implementation. Section 3 presents experimental results and comparison with other similar image restoration methods. Finally, Sect. 4 concludes the paper.

2 Image restoration problem and proposed adaptive image restoration method

2.1 Image restoration problem

Let $u_0(\mathbf{x}), u(\mathbf{x}), v(\mathbf{x})$ be the original, restored, and corrupted grayscale images, respectively, where $\mathbf{x} = (x_1, x_2, \ldots, x_p) \in \Omega \subset \mathbb{R}^p$, $p = 1, 2, \ldots$ In this work, we only consider 2D images, i.e., $p = 2$, though the model can also be potentially utilized for higher dimensional data. The image restoration problem can be solved by the high-order total variation that has the following unconstrained minimization form [28,31]:

$$\arg\min_u \left\{ \int_\Omega |\nabla^q u|_2 d\mathbf{x} + \frac{\lambda}{2} \int_\Omega |\mathbf{K}u - v|_2^2 d\mathbf{x} \right\} \tag{1}$$

where λ is a positive regularization parameter, $\mathbf{K}$ is a filtering operator such as a linear blur operator. Operator ∇ is a derivative operator, and $\nabla^q = \nabla(\nabla^{(q-1)}u)$ is a $q-order$ derivative. In the case, the image is only degraded by noise, operator $\mathbf{K}$ is the identity operator $\mathbf{I}$. In this paper, we consider the norm $|\cdot|_2$ in L_2 space, and $\mathbf{K} \equiv \mathbf{I}$. If $q = 1$, the model (1) is a model for the image restoration problem by the first-order total variation. It is also well-known as the ROF model (Rudin–Osher–Fatemi):

$$\arg\min_u \left\{ \int_\Omega |\nabla u|_2 d\mathbf{x} + \frac{\lambda}{2} \int_\Omega |u - v|_2^2 d\mathbf{x} \right\} \tag{2}$$

The ROF model is effective to remove Gaussian noise. It preserves edges well. However, ROF cannot preserve geometry features of image and usually causes some artifacts such as staircasing artifact [28]. If $q = 2$, the model (1) is a model for image restoration by the second-order total variation:

$$\arg\min_u \left\{ \int_\Omega |\nabla^2 u|_2 d\mathbf{x} + \frac{\lambda}{2} \int_\Omega |u - v|_2^2 d\mathbf{x} \right\} \tag{3}$$

The model (3) preserves edges no better than (2), but it can eliminate artifacts [28]. This is a vital advantage of regularization by the high-order total variation. To combine advantages of both models (2) and (3), a combined model [28] with $\alpha > 0, \beta > 0$ can be considered as follows:

$$\arg\min_u \left\{ \alpha \int_\Omega |\nabla u|_2 d\mathbf{x} + \beta \int_\Omega |\nabla^2 u|_2 d\mathbf{x} + \frac{1}{2} \int_\Omega |u - v|_2^2 d\mathbf{x} \right\} \tag{4}$$

The model (4) is well-known as the TV-bounded Hessian model (TVBH). TVBH is shown to be effective in removing the Gaussian noise with preserving edges and eliminating artifacts associated with traditional TV type models. However, parameters estimation is a big challenge and the effectiveness of removing staircasing artifacts is dependent on selecting the robust parameters.

2.2 Proposed adaptive image restoration method

In model (4), if we consider that $\alpha = \beta/k, k > 0$, we obtain:

$$\arg\min_u \left\{ \beta \left(\int_\Omega |\nabla u|_2 d\mathbf{x} + k \int_\Omega |\nabla^2 u|_2 d\mathbf{x} \right) + \frac{k}{2} \int_\Omega |u - v|_2^2 d\mathbf{x} \right\}, \tag{5}$$

$$\arg\min_u \left\{ \int_\Omega |\nabla u|_2 d\mathbf{x} + k \int_\Omega |\nabla^2 u|_2 d\mathbf{x} + \frac{k}{2\beta} \int_\Omega |u - v|_2^2 d\mathbf{x} \right\}. \tag{6}$$

Let $\lambda = k/\beta$, we will acquire the following model:

$$\arg\min_u \left\{ \int_\Omega |\nabla u|_2 d\mathbf{x} + k \int_\Omega |\nabla^2 u|_2 d\mathbf{x} + \frac{\lambda}{2} \int_\Omega |u - v|_2^2 d\mathbf{x} \right\}. \tag{7}$$

The model (7) is called to be an adaptive image restoration model based on combining the first-order and the second-order total variations and $\lambda > 0$ is a parameter of data fidelity term, $k > 0$ is a balancing parameter between the first-order total variation (TV1) and the second-order total variation (TV2). The advantages of model (7) over model (4) are twofold: (i) parameter k in model (7) is a balancing parameter and plays a role as a prioritized choice for noise removal or artifacts elimination; and (ii) we can estimate the regularization parameter λ in model (7) easier than estimate parameters α and β in model (4). In practice, model (7) is easier to implement since we only need to set the priority for noise removal or artifacts elimination, see Sect. 2.3 for adaptively estimating this regularization parameter λ. To balance the effectiveness of noise removal, edge preservation, and artifacts elimination, we typically set $k = 1$. However, in the experiments, we will test several various cases of k as well.

One of the goals of this work is to focus on estimating the data fidelity parameter λ. This parameter is estimated based on multiscale parameter estimation with supporting inverse gradient calculations. To solve the model (7), there are several effective numerical implementations that are available in the optimization studies. In this work, we use the alternating direction method of multipliers that is related to the Bregman splitting method [11,28,31], due to its efficiency compared to other optimization techniques.

2.3 Multiscale estimation for regularization parameter

In [2,11], it is proved that the inverse-gradient-driven parameters will significantly improve the final denoising quality from corrupted images when used with the TV regularization. Following this success obtained from the previous adaptive TV models, here we choose the regularization parameter λ based on the inverse gradient:

$$\lambda(v) = \frac{\mu}{1 + \tau \max_\rho |G_\rho \star \nabla v|_2^2}, \tag{8}$$

where $G_\rho = \frac{1}{2\pi\rho^2} \exp\left(-\frac{x_1^2 + x_2^2}{2\rho^2}\right)$ is a 2D Gaussian kernel, the operator $\star$ is a 2D convolution, τ is a stabilizing constant (usually from 10^{-4} to 10^{-2}), $\mu = 2/9$ and we only consider scale parameter $\rho = 1, 2, 3, 4, 5$ (i.e., 5 scale-levels). Hence, model (7) can be rewritten in an explicit form as follows:

$$\arg\min_u \left\{ \int_\Omega |\nabla u|_2 d\mathbf{x} + k \int_\Omega |\nabla^2 u|_2 d\mathbf{x} + \frac{\lambda(v)}{2} \int_\Omega |u - v|_2^2 d\mathbf{x} \right\}. \tag{9}$$

With every value of scale parameter ρ, we acquire the corresponding value of expression $|G_\rho \star \nabla v|_2$. After evaluating all values of $|G_\rho \star \nabla v|_2$ in all of scales ρ, we will choose the maximum value $|G_\rho \star \nabla v|_2^2$. This value is used for estimating value of the regularization parameter λ with our model.

2.4 Numerical implementation

The alternating direction method of multipliers (ADMM) [11, 28,31] for the model (9) with adaptive parameter estimation is implemented as below. In the algorithm, parameter $\gamma > 0$ is a multiplier; w_1, w_2 are dual variables associated with u; b_1, b_2 are the Bregman parameters.

Step 1. Set initial values for the parameters $u^{[0]} = v, b_1^{[0]} = b_2^{[0]} = w_1^{[0]} = w_2^{[0]} = 0, \gamma = 10, k$.

Step 2. Estimate the parameter $\lambda(v)$ by multiscale.

Step 3. For each iteration step $r = 1, 2, 3, ...$

– Evaluate solutions by directions:

$$u^{[r+1]} = \arg\min_u \left\{ \frac{\lambda(v)}{2} |u - v|_2^2 + \frac{\gamma}{2} |b_1^{[r]} + \nabla u - w_1^{[r]}|_2^2 + k \frac{\gamma}{2} |b_2^{[r]} + \nabla^2 u - w_2^{[r]}|_2^2 \right\},$$

$$w_1^{[r+1]} = \arg\min_{w_1} \left\{ |w_1|_2 + \frac{\gamma}{2} |b_1^{[r]} + \nabla u^{[r+1]} - w_1|_2^2 \right\}, \tag{10}$$

$$w_2^{[r+1]} = \arg\min_{w_2} \left\{ k|w_2|_2 + \frac{\gamma}{2} |b_2^{[r]} + \nabla^2 u^{[r+1]} - w_2|_2^2 \right\}, \tag{11}$$

– Update the Bregman parameters:

$$b_1^{[r+1]} = b_1^{[r]} + \nabla u^{[r+1]} - w_1^{[r+1]}, \tag{12}$$

$$b_2^{[r+1]} = b_2^{[r]} + \nabla^2 u^{[r+1]} - w_2^{[r+1]}. \tag{13}$$

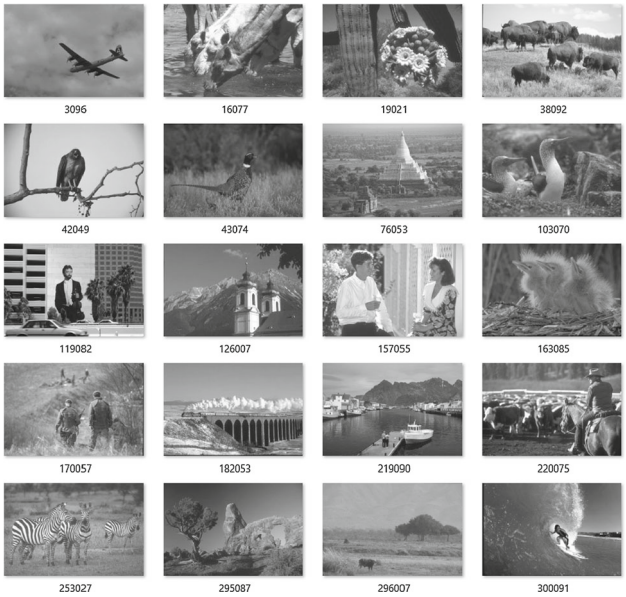

Fig. 1 The selected images of the UC Berkeley dataset for tests

Note that we can choose the stop condition based on the number of iteration steps or based on the tolerance. In this paper, we use the number of iteration.

3 Experimental results

3.1 Image dataset

We compare the performance of the proposed method with other related models on images of the UC Berkeley segmentation dataset (BSDS) [29]. All images are in grayscale and in the JPEG format. We show a representative set of 20 images of the dataset in Fig. 1. The images contain natural scenarios and artificial man-made buildings with multiscale edges and flat, and texture regions.

3.2 Image quality assessment metrics

To evaluate quality of images restored by the image restoration models, we utilize the peak signal-to-noise ratio (PSNR), the structural similarity (SSIM), the multiscale structural similarity (MS-SSIM), the features similarity (F-SIM), and the perceptual similarity (P-SIM) metrics that are widely used in the literature [9,10,12,32,33].

The peak signal-to-noise ratio PSNR is defined as:

$$\mathrm{PSNR} = 10\log_{10}\left(\frac{\omega_{\max}^2}{\mathrm{MSE}}\right)\mathrm{dB}, \tag{14}$$

with $\mathrm{MSE} = \frac{1}{mn}\sum_{i=1}^{m}\sum_{j=1}^{n}\left(\omega_1^{(ij)} - \omega_2^{(ij)}\right)^2$ is mean squared error with ω_{max} denoting the maximum grey value, for example, for 8-bit images $\omega_{max} = 255$; $\omega_1^{(ij)}, \omega_2^{(ij)}$ are gray values at every pixel location (i, j) of a given image ω_1 and a reference image (ground truth) ω_2, respectively; m and n are number of pixels by the image width and the image height, respectively. Note that the higher PSNR (measured in decibels - dB) indicates better image quality.

Structural similarity (SSIM) is a better error metric for comparing image quality, and its value is in the range of [0, 1] with value closer to one indicating better structure preservation. SSIM is evaluated based on the human visual system (HVS). SSIM of two images ω_1, ω_2 with a common size of $m \times n$ is defined as follows:

$$\mathrm{SSIM} = \frac{\left(2\mu_{\omega_1}\mu_{\omega_2} + c_1\right)\left(2\sigma_{\omega_1\omega_2} + c_2\right)}{\left(\mu_{\omega_1}^2 + \mu_{\omega_2}^2 + c_1\right)\left(\sigma_{\omega_1}^2 + \sigma_{\omega_2}^2 + c_2\right)} \tag{15}$$

where μ_{ω_i} is mean of ω_i, $\sigma_{\omega_i}^2$ is the variance of ω_i, $\sigma_{\omega_1\omega_2}$ is the covariance, and c_1, c_2 are stabilization parameters.

The multiscale structural similarity (MS-SSIM) [34] metric is similar to SSIM because it also bases on HVS. However, instead of using the single-scale approach, MS-SSIM is evaluated based on multiscale. Hence, MS-SSIM is more flexible than SSIM. Moreover, since MS-SSIM incorporates the variations of image resolution and viewing conditions, it is considered to be better than SSIM to evaluate image quality. MS-SSIM value is in the range of [0, 1], and the higher MS-SSIM indicates a better image quality.

Other image quality metrics based on HVS are the feature similarity (F-SIM) [35], the perceptual similarity (P-SIM) [36], the autoregressive image sharpness metric (ARISM) [37], the saliency-guided quality measure of screen content images (SQMS) [38], and the structural variation-based quality index (SVQI) [39]. F-SIM is evaluated based on salient low-level features: the phase congruency and the image gradient magnitude. They represent complementary aspects of the image visual quality. P-SIM is a combination of convolution operations at multiscales, gradient magnitude, color information similarity, and a perceptual-based pooling. Similar to SSIM, F-SIM and P-SIM values are in the range of [0, 1]. The higher F-SIM (or P-SIM) indicates a better image quality. In the article, we benchmark image quality based on PSNR, SSIM, MS-SSIM, F-SIM, and P-SIM.

3.3 Parameters setting

The implementation of the TVL, TVBH is undertaken using the guidelines provided by Lu and Duan [40]. All methods are implemented by the alternating direction method of multipliers. We use default parameters that were proposed by respective models. In particular, the parameters

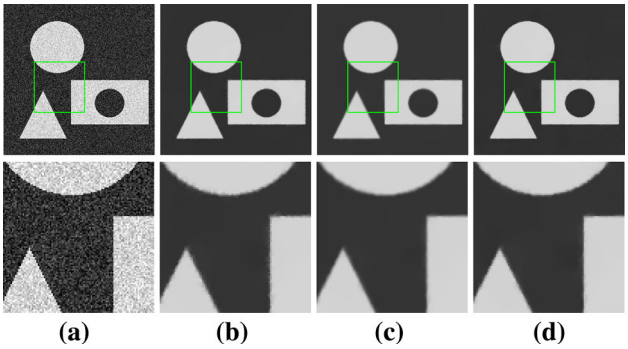

Fig. 2 Image restoration results for an artificial image with noise variance $\sigma = 0.2$. The denoising results with the values of PSNR, SSIM, MS-SSIM: **a** the noisy image, **b** TVL (13.8487/0.2691/0.9682), **c** TVBH with $TV1 : TV2 = 1 : 1$ (13.8528/0.2702/0.9687), **d** the proposed method with $k = 1$ (13.8762/0.2736/0.9691). N.b. Bottom row shows the close-up of the region shown in top row

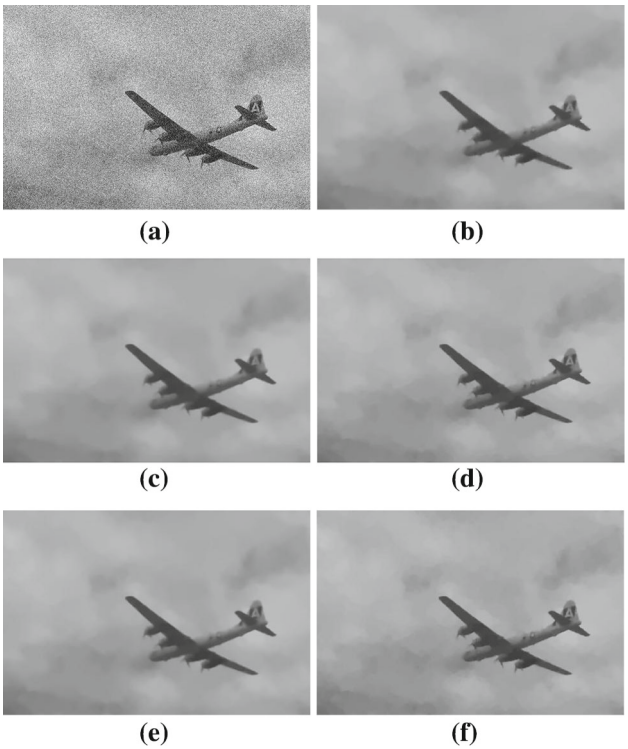

Fig. 3 The image restoration result for the plane image with ID 3096: **a** the noisy image, **b** Denoising by TVL, **c** Denoising by TVBH with proportion $TV1 : TV2 = 1$, **d** Denoising by TVBH with proportion $TV1 : TV2 = 2$, **e** Denoising by the proposed method with $k = 1$, **f** Denoising by the proposed method with $k = 1/2$

of TVL are $\alpha = 20, \beta = 10$, parameters of TVBH $1 : 1$ are $\alpha = 20, \beta = 20$, parameters of TVBH $2 : 1$ are $\alpha = 20, \beta = 10$. We set the number of iterations to 500. For the proposed method, we also use the same number of iterations being 500. We consider two test cases with various values of proportional parameter $k = 1$ (the weights of the first-order and the second-order total variations are the same)

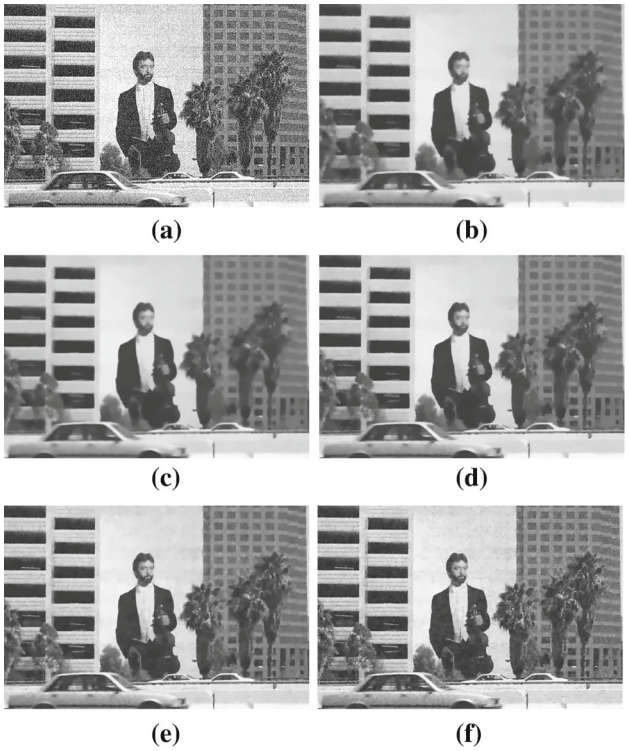

Fig. 4 The image restoration result for the poster of the violist image with ID 119082: **a** the noisy image, **b** Denoising by TVL, **c** Denoising by TVBH with proportion $TV1 : TV2 = 1$, **d** Denoising by TVBH with proportion $TV1 : TV2 = 2$, **e** Denoising by the proposed method with $k = 1$, **f** Denoising by the proposed method with $k = 1/2$

and $k = 1/2$ (the weight of the first-order total variation is twice the weight of the second-order total variation). For the constant τ in multiscale parameter estimation, we choose $\tau = 10^{-4}$.

3.4 Test cases and discussion

To generate noisy images, we add the Gaussian noise over original images by using the built-in *imnoise* function of MATLAB. For the first case of an artificial image, we use the Gaussian noise with zero mean and variance being 0.2. For the second case of natural images, we use the Gaussian noise with zero mean and variance being 0.1.

For the first test case, we made an artificial image with a black background containing a white disk, a black disk inside a white rectangle and a white triangle. Denoising results are presented in Fig. 2. The first row is for the full size of images, and the second row is for the cropped size of 100×100. We can see that all methods can preserve geometrical structures well. However, edges in the result of TVL are not preserved well. Edges in the result of TVBH $1 : 1$ are slightly blurred. The result of our method is the best. The PSNR, SSIM, and MS-SSIM values of the result of our method are also higher than ones of other methods.

Table 1 The values of PSNR of restored images by various methods

IDs	Noisy	TVL	TVBH 1:1	TVBH 2:1	Proposed $k = 1$	Proposed $k = 1/2$
103070	17.0392	19.2899	19.2388	19.3641	19.3841	19.5001
119082	17.235	18.2482	18.1808	18.5604	19.0024	19.1732
126007	17.1264	19.2695	19.2192	19.3893	19.4526	19.5903
157055	17.5841	18.9890	18.8962	19.1882	19.4326	19.6640
16077	17.297	19.0838	18.9992	19.2093	19.3549	19.5146
163085	16.9803	19.1168	19.0568	19.2018	19.2025	19.3351
170057	17.0078	19.1565	19.0941	19.2491	19.3447	19.4632
182053	17.2124	18.2661	18.1761	18.5016	18.7719	19.0597
219090	17.0695	18.8851	18.8195	19.0598	19.1025	19.3059
220075	17.1682	18.9391	18.8651	19.1463	19.4212	19.5057
253027	17.1651	17.7893	17.6794	18.2084	18.9752	19.1088
19021	17.1235	18.7917	18.7138	18.9455	19.1259	19.2960
295087	16.9852	18.8558	18.7983	18.9446	18.9509	19.1189
296007	16.9723	19.5260	19.5016	19.5461	19.5221	19.5675
300091	17.0934	19.2227	19.1771	19.3218	19.3195	19.4581
3096	17.0086	19.8542	19.8505	19.8821	19.8638	19.8937
38092	17.7167	19.1662	19.0859	19.3032	19.5094	19.7163
42049	17.4054	19.8159	19.7802	19.9614	20.0249	20.0897
43074	17.0055	19.2720	19.2353	19.3325	19.3159	19.4230
76053	17.0388	19.1529	19.1025	19.2378	19.2406	19.3743
Average:	17.1617	19.0345	18.9735	19.1777	19.3159	19.4579

Table 2 The values of SSIM of restored images by various methods

IDs	Noisy	TVL	TVBH 1:1	TVBH 2:1	Proposed $k = 1$	Proposed $k = 1/2$
103070	0.27731	0.7020	0.6880	0.7210	0.7276	0.7596
119082	0.46193	0.5674	0.5552	0.6105	0.6895	0.7169
126007	0.26609	0.7142	0.7044	0.7337	0.7461	0.7720
157055	0.3995	0.6481	0.6337	0.6783	0.7209	0.7547
16077	0.39277	0.5971	0.5808	0.6229	0.6568	0.7012
163085	0.28971	0.6662	0.6515	0.6871	0.6871	0.7240
170057	0.29373	0.6560	0.6373	0.6786	0.7114	0.7507
182053	0.40196	0.6742	0.6606	0.7048	0.7442	0.7679
219090	0.30261	0.6655	0.6561	0.6866	0.6941	0.7254
220075	0.34695	0.7170	0.7063	0.7392	0.7786	0.7626
253027	0.40163	0.6016	0.5859	0.6385	0.7321	0.7070
19021	0.3741	0.5857	0.5699	0.6120	0.6545	0.6984
295087	0.31772	0.6035	0.5891	0.6243	0.6257	0.6739
296007	0.21149	0.7064	0.6996	0.7165	0.7057	0.7254
300091	0.25211	0.6722	0.6629	0.6858	0.6858	0.7143
3096	0.12494	0.9317	0.9317	0.9338	0.9331	0.9338
38092	0.43237	0.5925	0.5767	0.6151	0.6634	0.7221
42049	0.23364	0.8995	0.8966	0.9103	0.9151	0.9022
43074	0.22673	0.6636	0.6531	0.6771	0.6745	0.7048
76053	0.31212	0.5742	0.5584	0.5980	0.5982	0.6478
Average:	0.316	0.6719	0.6599	0.6937	0.7172	0.7432

Table 3 The values of F-SIM of restored images by various methods

IDs	Noisy	TVL	TVBH 1:1	TVBH 2:1	Proposed $k = 1$	Proposed $k = 1/2$
103070	0.61981	0.80081	0.78346	0.81701	0.82395	0.85944
119082	0.72628	0.74541	0.73073	0.77233	0.84642	0.87423
126007	0.64398	0.75649	0.74411	0.77447	0.79305	0.83322
157055	0.70279	0.76346	0.74913	0.78408	0.82301	0.85615
16077	0.73492	0.73911	0.7219	0.75752	0.79296	0.83581
163085	0.62603	0.76263	0.74232	0.78106	0.78232	0.82456
170057	0.68619	0.73548	0.71368	0.7544	0.79196	0.84203
182053	0.76217	0.6851	0.66456	0.71096	0.76959	0.82178
219090	0.72436	0.71189	0.69261	0.73267	0.78278	0.8332
220075	0.67627	0.75148	0.7371	0.76887	0.78216	0.82566
253027	0.68194	0.83112	0.81993	0.84568	0.88512	0.89025
19021	0.72898	0.71229	0.69066	0.74958	0.85719	0.86926
295087	0.69573	0.65859	0.63809	0.67961	0.68686	0.74562
296007	0.61173	0.71831	0.70531	0.73081	0.71622	0.74629
300091	0.66576	0.72353	0.70983	0.73765	0.74007	0.7787
3096	0.33323	0.93769	0.93563	0.93862	0.93817	0.94034
38092	0.7721	0.69461	0.67747	0.71297	0.76995	0.82829
42049	0.49976	0.90091	0.89637	0.90772	0.91425	0.90933
43074	0.53944	0.76753	0.75135	0.78157	0.78027	0.81831
76053	0.69972	0.68461	0.66233	0.70752	0.7105	0.76757
Average:	0.65656	0.75405	0.73833	0.77226	0.79934	0.835

Table 4 The average values of the HVS-based metrics (SSIM, MS-SSIM, F-SIM, P-SIM) of the methods

Metric	TVL	TVBH 1:1	TVBH 2:1	Proposed $k = 1$	Proposed $k = 1/2$
SSIM	0.6719	0.6599	0.6937	0.7172	0.7432
MS-SSIM	0.88198	0.8718	0.89421	0.90985	0.92178
F-SIM	0.75405	0.73833	0.77226	0.79934	0.835
P-SIM	0.99789	0.99767	0.99817	0.99838	0.99862

For the second test case, we test on natural images. The denoising results for the plane image (ID 3096), for the poster of the violinist image (ID 119082), and for the surfer image (ID 300092) are presented in Figs. 3, 4, and 5, respectively.

Closer inspection of the different image restoration models on the plane images of Fig. 3 indicates that details of the plane in the case of TVL are not preserved, especially details on the border (edges) of the plane, including the symbol A on the plane tail being blurred. In the case of TVBH, with proportion 1 : 1, the image is too smooth; with proportion 2 : 1, the restoration result looks better. Our method gives a better result than other methods overall in terms of edge preservation and devoid of artifacts associated with TV type models. In the case of $k = 1$, the restored image is less blurred than TVBH with proportion 1 : 1 and in the case of $k = 1/2$, details of the restored image are clearer than TVBH with proportion 2 : 1. By PSNR and SSIM metrics, the proposed method with $k = 1$ is better than TVL, TVBH 1 : 1 and with $k = 1/2$ gives the best restoration result.

For the poster of the violinist image, the restoration results by TVL, TVBH 1 : 1, and TVBH 2 : 1 are blurred at edges and flat regions contain staircasing artifacts. The details of the face (especially, eyes) of the violinist are blurred, and the horizontal lines on walls of the left building are completely lost in the restoration results. In contrast, our proposed method gives a better restoration result with good features preservation. We note that all major edges are preserved well, including the building and windows edges. In the case of $k = 1$, artifacts were removed perfectly. For the case of $k = 1/2$, the details look the best; however, artifacts elimination is not perfect. In this case, by PSNR and SSIM metrics, the proposed method with $k = 1/2$ gives the best result, followed by the proposed method with $k = 1$.

For the surfer image, the restoration results are similar to the case of the plane image. Details of the restored image by our method with $k = 1/2$ are the best preserved. PSNR and SSIM values of our method, in this case, are the highest.

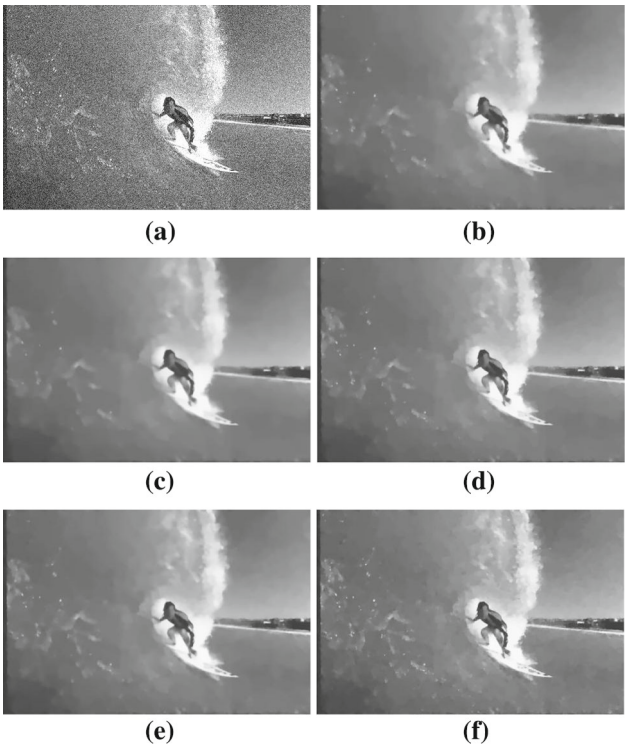

Fig. 5 The image restoration result for the surfer image with ID 300091: **a** the noisy image, **b** Denoising by TVL, **c** Denoising by TVBH with proportion $TV1 : TV2 = 1$, **d** Denoising by TVBH with proportion $TV1 : TV2 = 2$, **e** Denoising by the proposed method with $k = 1$, **f** Denoising by the proposed method with $k = 1/2$

Table 1 presents the PSNR values of the methods. The proposed method with $k = 1/2$ gives the best result and followed by the proposed method with $k = 1$. There are only four cases (IDs 296007, 300091, 3096, 43074), the PSNR values of the proposed method with $k = 1$ are lower than ones of TVBH $2 : 1$, but still higher than ones of TVL and TVBH $1 : 1$. Table 2 presents the SSIM values. The proposed method with $k = 1$ and $k = 1/2$ also gives better results than others. The proposed method with $k = 1/2$ gives the best result in most cases, followed by the proposed method with $k = 1$. The F-SIM values are presented in Table 3. Table 4 presents the average values of the HVS-based metrics such as SSIM, MS-SSIM, F-SIM, and P-SIM of the methods for 20 images of the BSDS dataset [29]. As can be seen, the scores of our method are always higher than ones of others.

Based on the comparison of the restoration results, we observed that our method is better qualitatively as well in quantitatively across standard image quality metrics such as PSNR, SSIM, MS-SSIM, F-SIM, and P-SIM. The results are seen clearly in Fig. 6. We implemented all methods on the same numerical solution method—the alternating direction method of multipliers, and we used the same setting for the parameters, the difference of time execution is very small and can be skipped. To process an image of size 1024×1024, all methods only take up to 3 s.

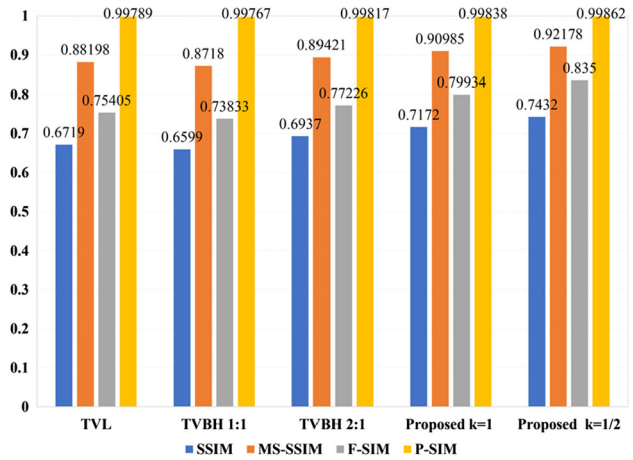

Fig. 6 The average values of the HVS-based metrics (SSIM, MS-SSIM, F-SIM, P-SIM) of the methods

4 Conclusions

In this article, we have proposed an adaptive image restoration method based on a combination of the first-order and the second-order total variations with adaptive multiscale parameter estimation. This method utilizes advantages of noise removal and edge preservation of the first-order total variation, artifacts elimination of the second-order total variation and of adaptive multiscale parameter estimation. In the implementation of the proposed method, we only need to set a positive value for parameter k to give priority of the first-order total variation or the second-order total variation in the restoration process. If $k > 1$, priority is for artifacts elimination. If $0 < k < 1$, priority is for noise removal. To balance the performance of noise removal and artifact elimination, we can set $k = 1$. Based on the comparison of the restoration results from different related models, we can confirm that the proposed method is better qualitatively as well as quantitatively in standard image quality metrics such as the PSNR, SSIM, MS-SSIM, F-SIM, and P-SIM. We obtained the image quality metrics values with our proposed method (19.3159, 0.7172, 0.90985, 0.79934, 0.99838), whereas other models such as the TV-Bounded Hessian (TVBH) (18.9735, 0.6599, 0.8718, 0.73833, 0.99767), and TV-Laplacian (TVL) (19.0345, 0.6719, 0.88198, 0.75405, 0.99789) indicating the superior restorations. The execution time of the proposed method is equivalent to TVBH and TVL models.

References

1. Cheng, J., Gao, Y., Guo, B., Zuo, W.: Image restoration using spatially variant hyper-Laplacian prior. Signal Image Video Process **13**(1), 155–162 (2019)
2. Prasath, V.B.S., Vorotnikov, D., Pelapur, R., Jose, S., Seetharaman, G., Palaniappan, K.: Multiscale Tikhonov-total variation image

restoration using spatially varying edge coherence exponent. IEEE Trans. Image Process. **24**(12), 5220–5235 (2015)
3. Chan, T.F., Shen, J.: Image Processing and Analysis: Variational, PDE, Wavelet and Stochastic Methods. SIAM, New York (2005)
4. Thanh, D.N.H., Dvoenko, S.: A variational method to remove the combination of poisson and Gaussian noises. In: 5th International Workshop on Image Mining: Theory and Applications, pp. 38–45, Germany (2015)
5. Shi, Y., Wang, K., Chen, C., Xu, L., Lin, L.: Structure-preserving image super-resolution via contextualized multitask learning. IEEE Trans. Multimedia. **19**(12), 2804–2815 (2017). https://doi.org/10.1109/TMM.2017.2711263
6. Liu, L., Pang, Z.-F., Duan, Y.: Retinex based on exponent-type total variation scheme. Inverse Prob. Imaging. **12**(5), 1199–1217 (2018). https://doi.org/10.3934/ipi.2018050
7. Liu, P., Zhang, H., Zhang, K., Lin, L., Zuo, W.: Multi-level wavelet-CNN for image restoration. In: Proceedings of 2018 IEEE/CVF Conference on Computer Vision and Pattern Recognition Workshops (CVPRW). Salt Lake city (2018). https://doi.org/10.1109/CVPRW.2018.00121
8. Fu, B., Li, Y., Wang, X.-H., Ren, Y.-G.: Image super-resolution using TV priori guided convolutional network. Pattern Recogn. Lett. **125**, 780–784 (2019). https://doi.org/10.1016/j.patrec.2019.06.022
9. Thanh, D.N.H., Prasath, V.B.S., Hieu, L.M.: A review on CT and X-ray images denoising methods. Informatica **43**(2), 151–159 (2019)
10. Thanh, D.N.H., Dvoenko, S.: Image noise removal based on total variation. Comput. Opt. **39**(4), 564–571 (2015)
11. Prasath, V.B.S.: Quantum noise removal in X-ray images with adaptive total variation regularization. Informatica **28**(3), 505–515 (2017)
12. Thanh, D.N.H., Dvoenko, S.: A method of total variation to remove the mixed Poisson–Gaussian noise. Pattern Rec. Image Ana. **26**(2), 285–293 (2016)
13. Mamaev, N.V., Yurin, D.V., Krylov, A.S.: Finding the parameters of a nonlinear diffusion denoising method by ridge analysis. Comput. Math. Model. **29**, 334–343 (2018). https://doi.org/10.1007/s10598-018-9413-6
14. Dovganich, A.A., Krylov, A.S.: A nonlocal image denoising algorithm using the structural similarity metric. Program. Comput. Soft. **45**, 141–146 (2019). https://doi.org/10.1134/S0361768819040029
15. Pang, Z.-F., Zhang, H.-L., Luo, S., Zeng, T.: Image denoising based on the adaptive weighted TVp regularization. Signal Process. **167**, 107325 (2020). https://doi.org/10.1016/j.sigpro.2019.107325
16. Teoh, S.H., Ibrahim, H.: Robust algorithm for broad impulse noise removal utilizing intensity distance and intensity height methodologies. SIViP **8**, 223–242 (2014). https://doi.org/10.1007/s11760-013-0538-y
17. Erkan, U., Enginoglu, S., Thanh, D.N.H., Hieu, L.M.: Adaptive frequency median filter for the salt-and-pepper denoising problem. IET Image Process. (2019). https://doi.org/10.1049/iet-ipr.2019.0398
18. Chen, Y., et al.: Structure-adaptive fuzzy estimation for random-valued impulse noise suppression. IEEE. Trans. Circ. Syst. Video Technol. **28**(2), 414–427 (2018). https://doi.org/10.1109/TCSVT.2016.2615444
19. Hsieh, P.-W., Shao, P.-C., Yang, S.-Y.: A regularization model with adaptive diffusivity for variational image denoising. Signal Process. **149**, 214–228 (2018). https://doi.org/10.1016/j.sigpro.2017.12.011
20. Erkan, U., Thanh, D.N.H., Hieu, L.M., Enginoglu, S.: An iterative mean filter for image denoising. IEEE Access. **7**, 167847–167859 (2019). https://doi.org/10.1109/ACCESS.2019.2953924
21. Almeida, M., Almeida, L.: Blind and semi-blind deblurring of natural images. IEEE Trans. Image Process. **19**(1), 36–52 (2009)
22. Abbass, M., Kim, H., Abdelwahab, S., Haggag, S., El-Rabaie, E., Dessouky, M., El-Samie, F.: Image deconvolution using homomorphic technique. Signal Image Video Process. **13**(4), 703–709 (2019)
23. Thanh, D.N.H., Prasath, V.B.S., Son, N.V., Hieu, L.M.: An adaptive image inpainting method based on the modified Mumford–Shah model and multiscale parameter estimation. Comput. Opt. **42**(6), 251–257 (2018)
24. Mirkamali, M., Nagabhushan, P.: Object removal by depth-wise image inpainting. Signal Image Video Process. **9**(8), 1785–1794 (2015)
25. Wang, W., Yuan, X.: Recent advances in image dehazing. IEEE/CAA J Automatica Sinica **4**(3), 410–436 (2017)
26. Grigoras, R., Ciocoiu, I.B.: Comparative analysis of deraining algorithms. In: International Symposium on Signals, Circuits and Systems, Romania (2017)
27. Rudin, L., Osher, S., Fatemi, E.: Nonlinear total variation based noise removal algorithms. Physica D **60**, 259–268 (1990)
28. Papafitsoros, K., Schönlieb, C.: A combined first and second order variational approach for image reconstruction. J Math. Imag. Vis. **48**(2), 308–338 (2014)
29. Arbelaez, P., Fowlkes, C., Martin, D.: The Berkeley Segmentation Dataset (BSDS). https://www2.eecs.berkeley.edu/Research/Projects/CS/vision/bsds/. Accessed 10/12/2018
30. Chan, R., Liang, H., Wei, S., Nikolova, M., Tai, X.: High-order total variation regularization approach for axially symmetric object tomography from a single radiograph. Inverse Prob. Imag. **9**(1), 55–77 (2015)
31. Lu, W., Duan, J., Qiu, Z., Pan, Z., Liu, R.W., Bai, L.: Implementation of high-order variational models made easy for image processing. Math. Meth. Appl. Sci. **39**(14), 4208–4233 (2016)
32. Thanh, D.N.H., Thanh, L.T., Hien, N.N., Prasath, V.B.S.: Adaptive Total Variation L1 Regularization for Salt and Pepper Image Denoising. Optik-Int. J. Light Electron Opt. (2020). https://doi.org/10.1016/j.ijleo.2019.163677
33. Wang, Z., Bovik, A., Sheikh, H., Simoncelli, E.: Image quality assessment: from error visibility to structural similarity. IEEE Trans. Image Process. **13**(4), 600–612 (2004)
34. Wang, Z., Simoncelli, E., Bovik, A.: Multi-scale structural similarity for image quality assessment. In: 37th IEEE Asilomar Conference on Signals, Systems and Computers, USA (2003)
35. Zhang, L., Zhang, L., Mou, X., Zhang, D.: FSIM: a feature similarity index for image quality assessment. IEEE Trans. Image Process. **20**(8), 2378–2386 (2011)
36. Gu, K., Li, L., Lu, H., Min, X., Lin, W.: A fast reliable image quality predictor by fusing micro-and macro-structures. IEEE Trans. Ind. Electron. **64**(5), 3903–3912 (2017)
37. Gu, K., Zhai, G., Lin, W., Yang, X., Zhang, W.: No-reference image sharpness assessment in autoregressive parameter space. IEEE Trans. Image Process. **24**(10), 3218–3231 (2015)
38. Gu, K., Wang, S., Yang, H., Lin, W., Zhai, G., Yang, X., Zhang, W.: Saliency-guided quality assessment of screen content images. IEEE Trans. Multimed. **18**(6), 1098–1110 (2016)
39. Gu, K., Qiao, J., Min, X., Yue, G., Lin, W., Thalmann, D.: Evaluating quality of screen content images via structural variation analysis. IEEE Trans. Vis. Comput. Graph. **24**(10), 2689–2701 (2017)
40. Lu, W., Duan, J.: Higher order variational models (HOVM) for image processing. https://github.com/j-duan/HOVM. Accessed 10/12/2018